

Silicon-Phosphorene Nanocavity-Enhanced Optical Emission at Telecommunications Wavelengths

Chad Husko,^{*,†} Jooheon Kang,^{‡,⊥} Gregory Moille,^{§,#} Joshua D. Wood,[‡] Zheng Han,^{§,▽} David Gosztola,[†] Xuedan Ma,[†] Sylvain Combré,^{||} Alfredo De Rossi,^{||} Mark C. Hersam,[‡] Xavier Checoury,[§] and Jeffrey R. Guest[†]

[†]Center for Nanoscale Materials, Argonne National Laboratory, Argonne, Illinois 60439, United States

[‡]Department of Materials Science and Engineering, Northwestern University, Evanston, Illinois 60208, United States

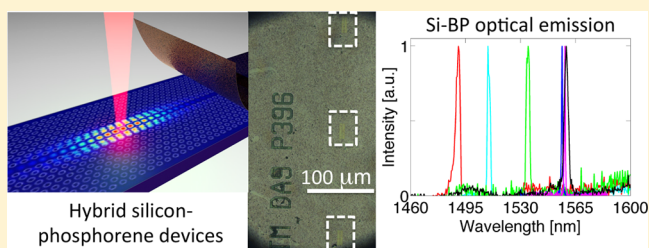
[§]Centre de Nanosciences et de Nanotechnologies, CNRS, Université Paris-Sud, Université Paris-Saclay, Bât. 220, 91405 Orsay cedex, France

^{||}Thales Research and Technology, 1 Av. A. Fresnel 128, 91767 Palaiseau, France

Supporting Information

ABSTRACT: Generating and amplifying light in silicon (Si) continues to attract significant attention due to the possibility of integrating optical and electronic components in a single material platform. Unfortunately, silicon is an indirect band gap material and therefore an inefficient emitter of light. With the rise of integrated photonics, the search for silicon-based light sources has evolved from a scientific quest to a major technological bottleneck for scalable, CMOS-compatible, light sources. Recently, emerging two-dimensional materials have opened the prospect of tailoring material properties based on atomic layers. Few-layer phosphorene, which is isolated through exfoliation from black phosphorus (BP), is a great candidate to partner with silicon due to its layer-tunable direct band gap in the near-infrared where silicon is transparent. Here we demonstrate a hybrid silicon optical emitter composed of few-layer phosphorene nanomaterial flakes coupled to silicon photonic crystal resonators. We show single-mode emission in the telecommunications band of $1.55\ \mu\text{m}$ ($E_g = 0.8\ \text{eV}$) under continuous wave optical excitation at room temperature. The solution-processed few-layer BP flakes enable tunable emission across a broad range of wavelengths and the simultaneous creation of multiple devices. Our work highlights the versatility of the Si-BP material platform for creating optically active devices in integrated silicon chips.

KEYWORDS: silicon photonics, nanomaterials, phosphorene, silicon optical emission, two-dimensional materials, nanophotonics



In the past decade, silicon photonics has reached a level of maturity where foundries are able to produce complex circuits involving both optical and electronic components on a monolithic platform.¹ Various approaches to create silicon-based lasers and light sources have been demonstrated.^{2–6} One approach considered for lasing in commercial silicon photonic circuits involves heterogeneous structures in which a direct-gap III–V wafer is bonded and then processed on top of a passive silicon circuit.⁷ Clever techniques to grow III–V gain media on silicon are also rapidly evolving.^{8–10} Further integration and simplification would be achieved with a gain material that can be deposited directly on silicon which uses the silicon itself as the optical resonator.

In this regard, the rise of two-dimensional (2D) materials offers a new route to take established material platforms beyond their intrinsic limitations. These thin van der Waals materials have been shown to exhibit layer-tunable luminescence^{11,12} and absorption,¹³ as well as large carrier mobility.¹⁴ Phosphorene has attracted particular interest for infrared optoelectronic devices,^{14,15} including photodetectors¹⁶ and

saturable absorbers in mode-locked lasers.¹⁷ Indeed, recent studies coupling 2D materials to photonic devices point to the advantages of hybrid material platforms.^{18,19} While earlier work focused on visible wavelength emission, more recent demonstrations show near-infrared optical emission at 1132²⁰ and 1305 nm²¹ utilizing two-dimensional MoTe₂ on silicon nanophotonic resonators. The development of silicon-compatible optical emitters deeper in the infrared would open up applications in telecommunications. Here, we utilize the direct band gap of few-layer phosphorene to functionalize silicon photonic crystal resonators and demonstrate optical emission in the telecommunications 1550 nm window. We leverage the layer-tunable optical gap of the BP to show emission across a broad 70 nm range. Our solution-processed synthesis method enables the creation of multiple devices in a single deposition step, highlighting the potential for scalability.

Received: July 25, 2018

Revised: September 6, 2018

Published: September 25, 2018

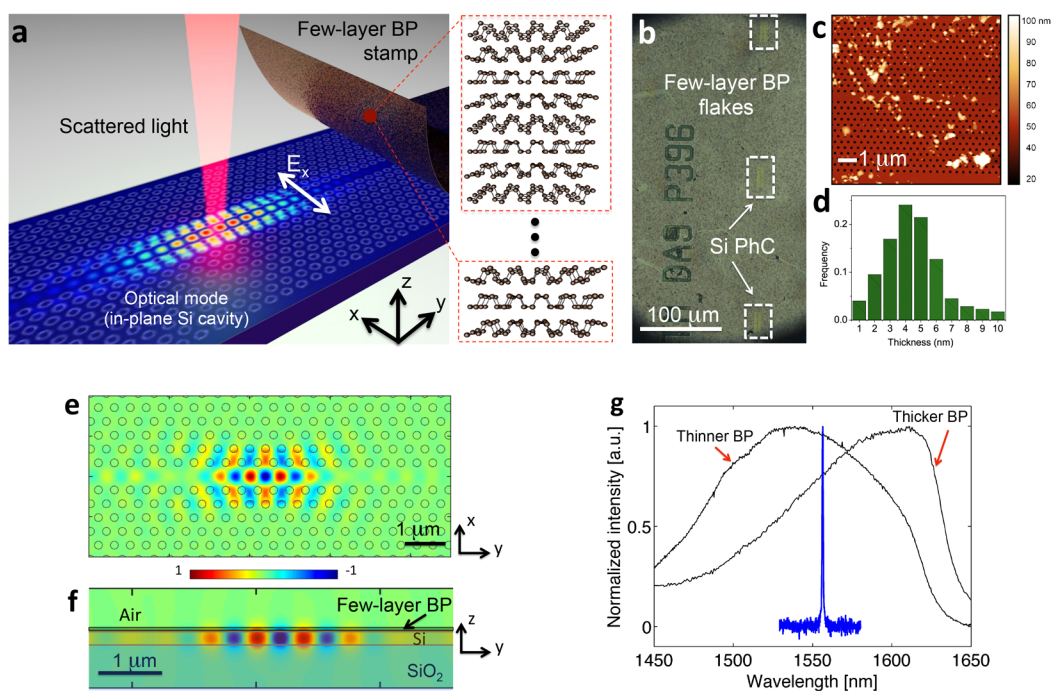


Figure 1. Hybrid Si-BP nanoscale light emitters. (a) Schematic of the hybrid silicon-phosphorene device. Light emitted from the few nanometer BP flakes is coupled to the silicon optical resonator (thickness 220 nm). The fundamental mode of the cavity is in the x - y plane. We collect light scattered from the cavity in the z -direction. Inset, atomic structure of different thicknesses of few-layer BP. (b) Optical microscope image of our hybrid device. The BP flakes cover multiple PhC devices on the silicon chip. (c) Atomic force microscopy image of a hybrid device with silicon PhC and BP emitter material. (d) Thickness distribution of the nanomaterial flakes composing the BP layer measured by AFM. (e,f) FDTD simulation showing the optical resonator mode of near-diffraction limited volume in the x - y plane (e) and y - z plane (f). The evanescent field in the silicon resonator couples to the BP on the surface. (g) Scaled cavity emission spectrum (blue line) compared to native photoluminescence signal from the two different thickness distributions of the few-layer BP flakes (black lines).

Figure 1a shows a schematic overview of the hybrid device. The silicon photonic crystal contains a mode-gap cavity optimized specifically for a SiO_2 cladding layer.²² The SiO_2 allows for better thermal conductivity compared to a purely air-clad Si cavity. The fundamental mode of the cavity is in the x - y (substrate) plane. Photonic crystals are a powerful medium for realizing classical and quantum light emitters due to their large quality factors (Q) and near diffraction-limited mode volumes (V) which enhance the spontaneous emission rate through the Purcell effect scaling with Q/V . An increased Purcell effect leads to a large spontaneous emission factor β and ultimately to low-threshold light emission.²³

We synthesize the few-layer BP flakes via a liquid-phase process in a deoxygenated aqueous dispersion, followed by a dry transfer onto the PhC cavity with a PDMS stamp.²⁴ Our method of creating and depositing chemically pristine BP flakes enable a large number of devices to be created at once in contrast to mechanical exfoliation of single flakes. The light emitted from the BP couples to the silicon resonator, which in turn provides feedback to the BP emitter. In the experiments, we collect light scattered from the cavity in the z -direction, representing a tiny fraction of the in-plane light confined within the nanocavity.

We fabricated the PhC cavity using electron-beam lithography and standard nanofabrication techniques on a 220 nm thick silicon-on-insulator wafer. The device design follows earlier work by some of the coauthors.²² The air holes have nominal radius 100 nm at a 404 nm pitch. We employed a dry transfer method in order to ensure the BP does not enter the air holes. For the emission experiments, we used a

microscope photoluminescence setup with an Olympus 100 \times near-infrared objective (N.A. 0.8). To excite the hybrid devices, we optically pumped the devices with a 1310 nm (0.95 eV) continuous-wave diode laser so as to avoid absorption and heating in the silicon cavity ($E_g = 1.1$ eV). The pump and collection paths (z -direction) are perpendicular to the resonator (x - y plane). The pump and Si-BP device light signals are separated by a dichroic and long-pass filter before the device signal is sent to a 30 cm Acton spectrometer with either a 600 or 150 line/mm grating depending on the resolution required and detected on a TEC-cooled InGaAs camera. The sample is kept at room temperature (292 K) under vacuum (2×10^{-4} mTorr) to prevent oxidation of the BP flakes.²⁵ For the pump-dependent emission experiments, we included a polarization analyzer in the collection path set to maximize the cavity peak and reduce residual background from BP outside the cavity region. We do not compensate for the polarization efficiency of the spectrometer grating which varies between 65 and 95% at our wavelengths of interest. The incident intensity is determined from the measured power after the objective assuming a diffraction-limited spot and takes into account the known transmission through the vacuum window.

The recipe for the BP dispersion follows our earlier work.²⁴ Ten milliliters of the as-prepared BP dispersion is vacuum-filtered on 47 mm diameter anodic aluminum oxide (AAO) membranes with 20 nm pore size (WhatmanTM) in ambient conditions. Subsequently, the BP nanosheets on the membrane are rinsed with deoxygenated water to remove the sodium dodecyl sulfate (SDS). Before the BP nanosheets on the membrane are fully dried, the nanosheets are transferred to the

Si cavity substrates by a polymethylsiloxane (PDMS) stamp. To promote surface adhesion of the BP nanosheets, deoxygenated water is sprayed on the substrates prior to stamping. For a schematic of the deposition process see the Supporting Information. For the thickness frequency distribution measurements, a substrate with BP flakes was loaded on an Asylum Cypher AFM with Si cantilevers (290 kHz resonant frequency) and AFM images were obtained in tapping mode at a scanning rate of 0.8 Hz using a minimum of 512 pixels per line.

Figure 1b is an optical microscope image of our fabricated device. Note that the optical resonators are approximately $1 \mu\text{m}^2$ of the $26 \times 9 \mu\text{m}^2$ devices, whereas the BP flakes span the entire image and cover multiple cavity devices. Figure 1c is an atomic force microscopy (AFM) image of a hybrid Si-BP device composed of a PhC silicon slab with air holes and the BP emitter material. While larger clusters are present on the surface, we emphasize that the BP flakes cover the entire image, as evidenced by photoluminescence measurements of a higher-order cavity mode on the devices. These measurements are shown below with further details on the higher-order mode in the Supporting Information. Figure 1d shows the thickness frequency distribution of the few-layer BP flakes as determined by atomic force microscopy on a separate sample.²⁴ Figure 1e is a finite-difference time-domain (FDTD) simulation of the optical nanocavity showing the in-plane (x - y) fundamental resonator mode with mode volume $V = 1.8(\lambda/n)^3$ while Figure 1f shows a side cut (y - z plane). The mode-gap cavity confines light by small variation of the lattice parameters to create an optical defect resonator. Notice that the evanescent optical field extends outside of the silicon region, allowing the cavity to couple to the BP layers on its surface and the hybrid system to behave as a single material as seen by the optical field.

Throughout this work we excite the devices at room temperature (292 K) with a continuous-wave 1310 nm laser. This wavelength is below the band gap of silicon, thus avoiding free-carrier absorption in the resonator layer. We maintain the sample under vacuum in order to prevent degradation of the BP^{25–28} and observe no photoinduced degradation of the system throughout these experiments. It is also possible to employ a passivation coating or chemical modification to achieve a similar result.^{25,29} To highlight this point, we fabricated a completely different chip with a passivation layer and present measurements of these devices in the Supporting Information. Figure 1g compares normalized emission spectra from the cavity region (blue curve) to the native photoluminescence signal from the BP flakes (black curves). The two black curves represent BP emission at different locations on the sample off the PhC region. The variation between the curves is due to thickness variations of the few-layer BP and thus different emission wavelengths, as indicated in Figure 1d.¹²

In Figure 2a, we show the experimentally measured spectra as a function of incident pump intensity. We estimate the flakes absorb $\approx 4\%$ of the stated incident light based on measured values of few-layer BP at 1310 nm.¹³ A peak defined by the cavity is apparent at the about 10 kW/cm^2 (0.4 kW/cm^2 absorbed) and grows with increasing pump power. Figure 2b shows individual spectra (blue dots) fit with a Lorentzian line shape (solid magenta lines). Figure 2c shows the evolution of the spectral line widths (fwhm, full width at half-maximum) as a function of input pump intensity. The uncertainties are taken as the root mean square deviation of the fit. We estimate the

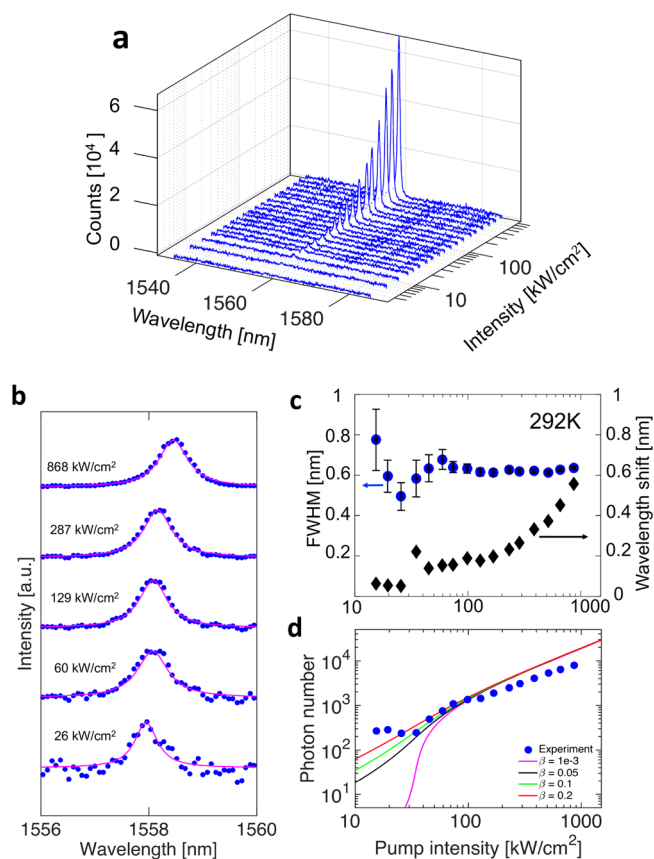


Figure 2. Experimental measurements at room temperature (292 K). (a) Background subtracted spectral evolution of the emission as a function of incident optical pump intensity. About 4% of the light is absorbed. (b) Individual spectra (blue dots) with Lorentzian fits to the cavity line shape (magenta). (c) Line width versus input pump intensity (blue dots) showing a nonmonotonic evolution. The line width increases due to gain-refractive index coupling before flattening out. Uncertainties are the RMS deviation of the fit. Below, the center wavelength of the resonance (black diamonds) undergoes a redshift, indicating the presence of thermal effects. (d) Cavity optical emission signal versus input pump intensity ($\text{Light}_{\text{in}} - \text{Light}_{\text{out}}$). The measured output spectra (blue dots) are compared to the rate equation model with different β factors (solid lines).

cold cavity Q with the BP on the surface to be on the order of 2000. This is lower than the design value of 50k, likely due to scattering and absorption from the BP. The emission line width first narrows as loss in the active region decreases before a slight broadening occurs due to gain-refractive index coupling. The line width evolution of nanoscale light emitters is complex due to competition between carrier and thermal effects and can exhibit nonmonotonic evolution.³⁰ A line width evolution similar to ours was demonstrated for PhC quantum well lasers.³¹ Following this work, we take the threshold for a possible lasing transition as $\approx 30 \text{ kW/cm}^2$ (1.2 kW/cm^2 absorbed). In Figure 2c, we also observe that the resonance spectrally redshifts above threshold, indicating the presence of thermal effects, possibly due to Auger recombination or free-carrier absorption.

Figure 2d shows the hybrid device emission signal versus input pump intensity, commonly called the “ $\text{Light}_{\text{in}} - \text{Light}_{\text{out}}$ ” ($L-L$) curve. The emitted signal (blue dots) is defined as the background-subtracted spectra integrated under the peak. The $L-L$ curve exhibits a nonlinear change in slope around 30 kW/cm^2

cm², corresponding to the line width evolution above and signifying the possible onset of stimulated emission. We solved the rate equations for various values of β to better understand the emission response (see [Supporting Information](#)). The output emission slightly rolls off above 100 kW/cm², which is consistent with the evolution of both the line width and the resonance shift, and provides further evidence for the thermal effects highlighted in [Figure 2c](#). Similar spectral shifts and intensity roll off have also been observed in quantum dot microdisk lasers.³²

We now discuss the localization of the light emission by comparing the BP emission at various spatial points on the sample. [Figure 3a](#) is an optical image showing the locations

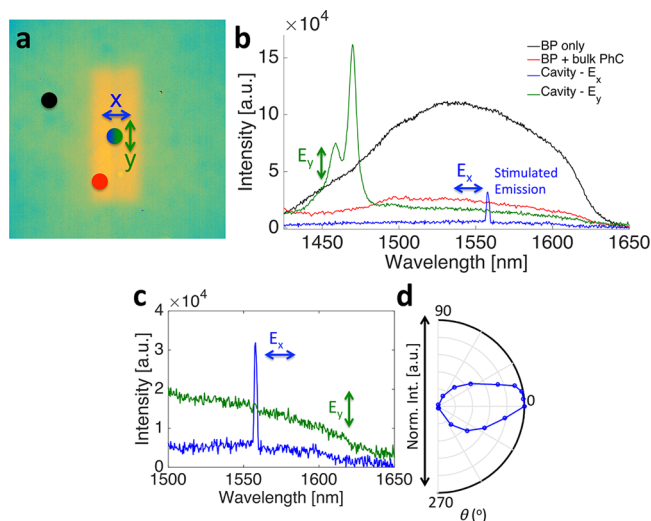


Figure 3. Spatial and polarization properties of the Si-BP device. (a) Optical image with the spatial points where we measured BP emission. The BP flakes cover the entire image. Legend: BP only (black, no polarizer), BP on bulk PhC (red, no polarizer), cavity optical emission (blue, polarizer 0° - E_x), resonator region with orthogonal polarization collection (green, polarizer 90° - E_y). (b) Spectra corresponding to (a) showing the different responses of the BP emission depending on the local photonic density of states. (c) Zoom image of the polarized emission spectra from the cavity region with the polarization analyzer set to orthogonal positions with the low-resolution grating. (d) Polar plot of the cavity emission spectra.

where we excited the BP flakes. While the underlying silicon has different structure (plain silicon, photonic crystal, or cavity region), the BP flakes covers the entire image. Thus, at each point we probe the effect of the local photonic density of states on the BP emission. [Figure 3b](#) illustrates the spectra captured at a pump intensity of 385 kW/cm². Both the BP emission on the unstructured silicon (black curve, no polarization analyzer) and the BP on the bulk PhC (red curve, no polarization analyzer) exhibit broad emission. However, when we pump the cavity region (blue curve, polarizer -0° - E_x), we notice that the emission spectrum is much narrower than the BP on either the plain or structured surfaces. This polarization direction is consistent with that expected from the fundamental mode of the cavity. We observe that the E_x cavity peak is greatly reduced when collecting the orthogonal polarization (green curve, 90° - E_y), as confirmed by the zoom view of the cavity response in [Figure 3c](#). The second green peak at 1470 nm is a higher-order mode (see [Supporting Information](#)). [Figure 3d](#) shows full polarization measurements of the cavity emission at

1558 nm. Though phosphorene exhibits anisotropic emission and absorption,^{13,33,34} the random orientation of the small flakes in our BP layer partially averages out this effect.

We investigated additional devices in the cavity resonator array to examine the bandwidth of the Si-BP emission, as well as to verify that the results are reproducible. [Figure 4a](#) is an

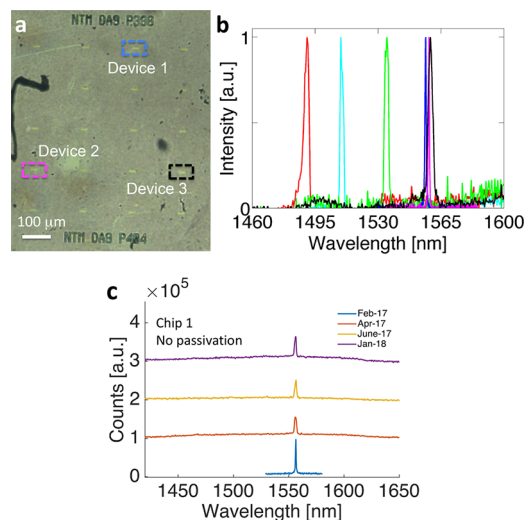


Figure 4. Demonstration of optical emission reproducibility and bandwidth. (a) Optical microscope image showing the devices in which we measured emission near 1550 nm. The properties of Device 1 are shown in the main text. (b) Normalized optical emission spectra from six different cavity emitters at 292 K. The emission range covers a 70 nm bandwidth, controlled by the cavity geometry, and is limited only by the designs on our current silicon chip. (c) Optical excitation measurements of the hybrid Si-BP devices over a 12 month period. The consistent emission level indicates material stability over time.

optical microscope image showing devices in which we measured emission centered in the important technological wavelength of 1550 nm. The detailed properties of Device 1 are described throughout the text. Simply by tuning the geometry of the silicon resonators, we further demonstrated that the emission wavelength can be continuously tuned over an ~70 nm wavelength range (1490–1560 nm), limited only by the designs on our current silicon chip. [Figure 4b](#) shows above-threshold spectra for six total emitters at 292 K, highlighting the versatility of this material system for broadband amplifiers and light-sources.

The stability of phosphorene has been widely studied in the literature.^{25–28} As described above, we performed the measurements under vacuum to avoid potential device degradation. In between measurement periods, we store the devices in a house nitrogen glovebox. To demonstrate the stability of our material platform, we measured the devices (Chip 1) spanning a period of approximately 12 months. [Figure 4c](#) shows emission measurements and a consistent level of emission over this time period. The narrower emission data from February 2017 corresponds to a higher-resolution grating as described in the main text. We note this is without a passivation coating and highlights the stability of the few-layer phosphorene nanomaterial flakes over time. As mentioned above, we fabricated a second chip with a passivation layer. We present the equivalent measurements to [Figure 4b](#) in the [Supporting Information](#) pumped under ambient conditions, highlighting both the robustness of the material under

passivation and demonstrating repeatability of the device fabrication procedure.

In summary, we reported optical emission from a hybrid nanostructure composed of a silicon optical resonator and a few-layer phosphorene emitting layer. While these experiments mark a first successful demonstration of light emission from this material combination, additional experiments are underway to further develop this platform for applications in integrated silicon optoelectronics. Since phosphorene is ambipolar, we anticipate electrical pumping is possible.^{14,35} We envision the few-layer BP dispersion used in this work could be processed in a residue-free solvent system³⁶ and further selectively sorted to have monodisperse flakes in thickness.³⁷ These solutions can be deposited directly onto the silicon resonators with standard nanofabrication and synthesis procedures, opening up the possibility of large-scale deployment of light emitters on a single chip. Further, while the small footprint and large- β of these nanoscale light emitters is useful, developing designs with larger BP gain regions are desirable for power scaling to match state-of-the-art integrated emitters.^{8,38} These results demonstrate that hybrid devices combining the light emitting properties of 2D phosphorene overcome the indirect band gap of silicon, opening a new route for CMOS-compatible light sources in integrated photonic chips.

■ ASSOCIATED CONTENT

■ Supporting Information

The Supporting Information is available free of charge on the ACS Publications website at DOI: 10.1021/acs.nanolett.8b03037.

Schematic of the BP nanosheets transfer, a rate equation model, lifetime measurements on the hybrid silicon-phosphorene device, photonic band structure and resonant optical modes, passivation techniques and device reproducibility (PDF)

■ AUTHOR INFORMATION

Corresponding Author

*E-mail: husko.physics@gmail.com.

ORCID

Chad Husko: 0000-0002-7125-2518

Jooheon Kang: 0000-0002-6578-2547

David Gosztola: 0000-0003-2674-1379

Mark C. Hersam: 0000-0003-4120-1426

Jeffrey R. Guest: 0000-0002-9756-8801

Present Addresses

[†](J.K.) Department of Chemistry, University of California, Berkeley, Berkeley, CA.

[#](G.M.) Center for Nanoscale Science and Technology, National Institute of Standards and Technology, Gaithersburg, Maryland. Maryland NanoCenter, University of Maryland, College Park, Maryland 20742

[∇](Z.H.) MirSense S.A., 8 Avenue de la Vauve, 91120 Palaiseau, France.

Author Contributions

C.H. and J.K. contributed equally to this work.

Notes

The authors declare the following competing financial interest(s): All of the work contained in the manuscript was carried out at the research institutions in the listed affiliations. In July of 2018, Chad Husko initiated a spin-out company

that targets the commercialization of the technology discussed in this work.

■ ACKNOWLEDGMENTS

This work was performed, in part, at the Center for Nanoscale Materials, a U.S. Department of Energy Office of Science User Facility and supported by the U.S. Department of Energy, Office of Science, under Contract No. DE-AC02-06CH11357, and Laboratory Directed Research and Development (LDRD) funding from Argonne National Laboratory, provided by the Director, Office of Science, of the U.S. Department of Energy under Contract No. DE-AC02-06CH11357. This work was also partly supported by the French RENATECH network. C.H. was supported by the Alexei Abrikosov Fellowship. The research collaboration between C.H. and X.C. was supported in part through the FACCTS Program (France and Chicago Collaborating in the Sciences) at the University of Chicago. J.K. and M.C.H. acknowledge support from National Science Foundation Grant DMR-1505849. The authors thank Andrew Mannix and Richard Schaller for helpful discussions.

■ REFERENCES

- (1) Sun, C.; Wade, M. T.; Lee, Y.; Orcutt, J. S.; Alloatti, L.; Georgas, M. S.; Waterman, A. S.; Shainline, J. M.; Avizienis, R. R.; Lin, S.; Moss, B. R.; Kumar, R.; Pavanello, F.; Atabaki, A. H.; Cook, H. M.; Ou, A. J.; Leu, J. C.; Chen, Y.-H.; Asanović, K.; Ram, R. J.; Popović, M. A.; Stojanović, V. M. Single-chip microprocessor that communicates directly using light. *Nature* **2015**, *528*, 534–538.
- (2) Fujii, M.; Yoshida, M.; Kanzawa, Y.; Hayashi, S.; Yamamoto, K. 1.54 μm photoluminescence of Er³⁺ doped into SiO₂ films containing Si nanocrystals: Evidence for energy transfer from Si nanocrystals to Er³⁺. *Appl. Phys. Lett.* **1997**, *71*, 1198–1200.
- (3) Pavesi, L.; Dal Negro, L.; Mazzoleni, C.; Franzò, G.; Priolo, F. Optical gain in silicon nanocrystals. *Nature* **2000**, *408*, 440–444.
- (4) Rong, H.; Jones, R.; Liu, A.; Cohen, O.; Hak, D.; Fang, A.; Paniccia, M. A continuous-wave Raman silicon laser. *Nature* **2005**, *433*, 725–728.
- (5) Camacho-Aguilera, R. E.; Cai, Y.; Patel, N.; Bessette, J. T.; Romagnoli, M.; Kimerling, L. C.; Michel, J. An electrically pumped germanium laser. *Opt. Express* **2012**, *20*, 11316.
- (6) Takahashi, Y.; Inui, Y.; Chihara, M.; Asano, T.; Terawaki, R.; Noda, S. A micrometrescale Raman silicon laser with a microwatt threshold. *Nature* **2013**, *498*, 470–474.
- (7) Fang, A. W.; Park, H.; Jones, R.; Cohen, O.; Paniccia, M. J.; Bowers, J. E. A continuous-wave hybrid AlGaInAs-Silicon evanescent laser. *IEEE Photonics Technol. Lett.* **2006**, *18*, 1143–1145.
- (8) Liang, D.; Bowers, J. E. Recent progress in lasers on silicon. *Nat. Photonics* **2010**, *4*, 511–517.
- (9) Wang, Z.; Tian, B.; Pantouvaki, M.; Guo, W.; Absil, P.; Van Campenhout, J.; Merckling, C.; Van Thourhout, D. Room-temperature InP distributed feedback laser array directly grown on silicon. *Nat. Photonics* **2015**, *9*, 837–842.
- (10) Chen, S.; Li, W.; Wu, J.; Jiang, Q.; Tang, M.; Shutts, S.; Elliott, S. N.; Sobiesierski, A.; Seeds, A. J.; Ross, I.; Smowton, P. M.; Liu, H. Electrically pumped continuous-wave III-V quantum dot lasers on silicon. *Nat. Photonics* **2016**, *10*, 307–311.
- (11) Mak, K. F.; Lee, C.; Hone, J.; Shan, J.; Heinz, T. F. Atomically thin MoS₂: A new direct-gap semiconductor. *Phys. Rev. Lett.* **2010**, *105*, 2–5.
- (12) Pei, J.; Gai, X.; Yang, J.; Wang, X.; Yu, Z.; Choi, D.-Y.; Luther-Davies, B.; Lu, Y. Producing air-stable monolayers of phosphorene and their defect engineering. *Nat. Commun.* **2016**, *7*, 10450.
- (13) Li, L.; Kim, J.; Jin, C.; Ye, G. J.; Qiu, D. Y.; da Jornada, F. H.; Shi, Z.; Chen, L.; Zhang, Z.; Yang, F.; Watanabe, K.; Taniguchi, T.; Ren, W.; Louie, S. G.; Chen, X. H.; Zhang, Y.; Wang, F. *Nat. Nanotechnol.* **2016**, *12*, 21–25.

- (14) Li, L.; Yu, Y.; Ye, G. J.; Ge, Q.; Ou, X.; Wu, H.; Feng, D.; Chen, X. H.; Zhang, Y. Black phosphorus field-effect transistors. *Nat. Nanotechnol.* **2014**, *9*, 372–377.
- (15) Xia, F.; Wang, H.; Jia, Y. Rediscovering black phosphorus as an anisotropic layered material for optoelectronics and electronics. *Nat. Commun.* **2014**, *5*, 4458.
- (16) Youngblood, N.; Chen, C.; Koester, S. J.; Li, M. Waveguide-integrated black phosphorus photodetector with high responsivity and low dark current. *Nat. Photonics* **2015**, *9*, 247–252.
- (17) Luo, Z.-C.; Liu, M.; Guo, Z.-N.; Jiang, X.-F.; Luo, A.-P.; Zhao, C.-J.; Yu, X.-F.; Xu, W.-C.; Zhang, H. Microfiber-based few-layer black phosphorus saturable absorber for ultra-fast fiber laser. *Opt. Express* **2015**, *23*, 20030.
- (18) Gu, T.; Petrone, N.; McMillan, J. F.; van der Zande, A.; Yu, M.; Lo, G. Q.; Kwong, D. L.; Hone, J.; Wong, C. W. Regenerative oscillation and four-wave mixing in graphene optoelectronics. *Nat. Photonics* **2012**, *6*, 554–559.
- (19) Wu, S.; Buckley, S.; Schaibley, J. R.; Feng, L.; Yan, J.; Mandrus, D. G.; Hatami, F.; Yao, W.; Vučković, J.; Majumdar, A.; Xu, X. Monolayer semiconductor nanocavity lasers with ultralow thresholds. *Nature* **2015**, *520*, 69–72.
- (20) Li, Y.; Zhang, J.; Huang, D.; Sun, H.; Fan, F.; Feng, J.; Wang, Z.; Ning, C. Z. Roomtemperature continuous-wave lasing from monolayer molybdenum ditelluride integrated with a silicon nanobeam cavity. *Nat. Nanotechnol.* **2017**, *12*, 987–992.
- (21) Fang, H.; Liu, J.; Li, H.; Zhou, L.; Liu, L.; Li, J.; Wang, X.; Krauss, T. F.; Wang, Y. 1305 nm Few-Layer MoTe₂-on-Silicon Laser-Like Emission. *Laser & Photonics Reviews* **2018**, *12*, 1800015.
- (22) Han, Z.; Chécoury, X.; Haret, L.-D.; Boucaud, P. High quality factor in a two-dimensional photonic crystal cavity on silicon-on-insulator. *Opt. Lett.* **2011**, *36*, 1749–1751.
- (23) Purcell, E. M. Spontaneous emission probabilities at radio frequencies. *Phys. Rev.* **1946**, *69*, 681.
- (24) Kang, J.; Wells, S. A.; Wood, J. D.; Lee, J.-H.; Liu, X.; Ryder, C. R.; Zhu, J.; Guest, J. R.; Husko, C. A.; Hersam, M. C. Stable aqueous dispersions of optically and electronically active phosphorene. *Proc. Natl. Acad. Sci. U. S. A.* **2016**, *113*, 11688–11693.
- (25) Wood, J. D.; Wells, S. a.; Jariwala, D.; Chen, K.-s.; Cho, E.; Sangwan, V. K.; Liu, X.; Lauthon, L. J.; Marks, T. J.; Hersam, M. C. Effective Passivation of Exfoliated Black Phosphorus Transistors Against Ambient Degradation. *Nano Lett.* **2014**, *14*, 6964–6970.
- (26) Favron, A.; Gaufres, E.; Fossard, F.; Phaneuf-L'Heureux, A.-L.; Tang, N. Y.-W.; Lévesque, P. L.; Loiseau, A.; Leonelli, R.; Francoeur, S.; Martel, R. Photooxidation and quantum confinement effects in exfoliated black phosphorus. *Nat. Mater.* **2015**, *14*, 826–832.
- (27) Island, J. O.; Steele, G. A.; Van Der Zant, H. S.; Castellanos-Gomez, A. Environmental instability of few-layer black phosphorus. *2D Mater.* **2015**, *2*, 011002.
- (28) Kim, J. S.; Liu, Y.; Zhu, W.; Kim, S.; Wu, D.; Tao, L.; Dodabalapur, A.; Lai, K.; Akinwande, D. Toward air-stable multilayer phosphorene thin-films and transistors. *Sci. Rep.* **2015**, *5*, 8989.
- (29) Ryder, C. R.; Wood, J. D.; Wells, S. A.; Yang, Y.; Jariwala, D.; Marks, T. J.; Schatz, G. C.; Hersam, M. C. Covalent functionalization and passivation of exfoliated black phosphorus via aryl diazonium chemistry. *Nat. Chem.* **2016**, *8*, 597–602.
- (30) Bjork, G.; Karlsson, A.; Yamamoto, Y. On the linewidth of microcavity lasers. *Appl. Phys. Lett.* **1992**, *60*, 304–306.
- (31) Matsuo, S.; Shinya, A.; Kakitsuka, T.; Nozaki, K.; Segawa, T.; Sato, T.; Kawaguchi, Y.; Notomi, M. High-speed ultracompact buried heterostructure photonic-crystal laser with 13 fJ of energy consumed per bit transmitted. *Nat. Photonics* **2010**, *4*, 648–654.
- (32) Wang, W. H.; Ghosh, S.; Mendoza, F. M.; Li, X.; Awschalom, D. D.; Samarth, N. Static and dynamic spectroscopy of (Al,Ga)-AsGaAs microdisk lasers with interface fluctuation quantum dots. *Phys. Rev. B: Condens. Matter Mater. Phys.* **2005**, *71*, 155306.
- (33) Qiao, J.; Kong, X.; Hu, Z.-X.; Yang, F.; Ji, W. High-mobility transport anisotropy and linear dichroism in few-layer black phosphorus. *Nat. Commun.* **2014**, *5*, 4475.
- (34) Liao, B.; Zhao, H.; Najafi, E.; Yan, X.; Tian, H.; Tice, J.; Minnich, A. J.; Wang, H.; Zewail, A. H. Spatial-Temporal Imaging of Anisotropic Photocarrier Dynamics in Black Phosphorus. *Nano Lett.* **2017**, *17*, 3675–3680.
- (35) Koenig, S. P.; Doganov, R. A.; Schmidt, H.; Castro Neto, A. H.; Özyilmaz, B. Electric field effect in ultrathin black phosphorus. *Appl. Phys. Lett.* **2014**, *104*, 103106.
- (36) Kang, J.; Wells, S. A.; Sangwan, V. K.; Lam, D.; Liu, X.; Luxa, J.; Sofer, Z.; Hersam, M. C. Solution-Based Processing of Optoelectronically Active Indium Selenide. *Adv. Mater.* **2018**, *30*, 1802990.
- (37) Kang, J.; Sangwan, V. K.; Wood, J. D.; Hersam, M. C. Solution-Based Processing of Monodisperse Two-Dimensional Nanomaterials. *Acc. Chem. Res.* **2017**, *50*, 943–951.
- (38) Crosnier, G.; Sanchez, D.; Bouchoule, S.; Monnier, P.; Beaudoin, G.; Sagnes, I.; Raj, R.; Raineri, F. Hybrid indium phosphide-on-silicon nanolaser diode. *Nat. Photonics* **2017**, *11*, 297–300.